

Integrated Time-Resolved Fluorescence and Diffuse Reflectance Spectroscopy Instrument for Intraoperative Detection of Brain Tumor Margin

Zhaojun Nie, Vinh Nguyen Du Le, *Student Member, IEEE*, Derek Cappon, John Provias, Naresh Murty, Joseph E. Hayward, Thomas J. Farrell, Michael S. Patterson, William McMillan, and Qiyin Fang

Abstract—Time-resolved fluorescence (TRF) and diffuse reflectance (DR) spectroscopy are two optical biopsy modalities that have been studied in tumor diagnosis. Combination of TRF and DR spectroscopy allows us to obtain more features such as fluorescence intensity, lifetime, and optical properties; thus, potentially improving the tissue diagnostic accuracy. In this paper, an integrated TRF-DR spectroscopy instrument was developed to acquire TRF spectra as well as spatially resolved diffuse reflectance spectra in sequence for intraoperative detection of brain tumor margin. The performance of TRF-DR spectroscopy instrumentation was calibrated and evaluated using endogenous biomolecules, tissue phantoms, and *ex vivo* brain tumor specimens. The results demonstrated that the TRF-DR system is capable to retrieve the fluorescence and optical properties accurately.

Index Terms—Time-resolved fluorescence, diffuse reflectance, spectroscopy, brain tumor margin, intraoperative detection.

I. INTRODUCTION

BRAIN and central nervous system (CNS) tumors were responsible for nearly 23 380 new cases and 14 320 deaths in the United States in 2014 [1]. Glioblastoma (or GBM) is a very aggressive type of tumor and account for 80% of malignant primary brain tumors [2]. Surgery is the most commonly prescribed treatment for malignant gliomas. The prognosis of

patients is directly correlated to the completeness of tumor removal during surgery [3]. Due to the infiltrative characteristics and morphological similarity to normal brain tissue, complete resection of malignant gliomas is difficult to achieve. The current “gold standard” for the diagnosis of tissue status in neurosurgery is excisional biopsy [4], which is time-consuming and unable to provide real-time diagnosis. In addition, for brain tissue biopsy, only limited samples can be resected to avoid damages to the normal brain, which may lead to sampling error.

To overcome these problems in biopsy, minimally invasive optical techniques, or optical biopsies, have been developed for intraoperative diagnosis. Fluorescence spectroscopy is one of common techniques used for tissue diagnosis. Endogenous fluorophores such as amino acids (tyrosine and tryptophan), structural proteins (elastin and collagen), and enzyme cofactors [e.g., reduced nicotinamide adenine dinucleotide (NADH) and flavin adenine dinucleotide (FAD)] can be potentially used to monitor the changes of biochemical compositions [5], intracellular and extracellular structures [6], [7], and metabolic status [8] occurring in tumor. Both fluorescence intensity and dynamic decay signals are utilized to characterize the variations in tumors [9]–[14]. In addition, diffuse reflectance spectroscopy has also been studied for tissue diagnosis. By collecting the diffuse reflectance light on the surface of biological tissue, it is capable to extract the absorption and scattering properties of the biological tissue, and further to estimate the biochemical (e.g., hemoglobin concentration [15]) and morphological (e.g., scatter size and shape) characteristics of biological tissue.

Combination of steady-state fluorescence and diffuse reflectance spectroscopy has been studied to diagnose brain tumor. The results show that it is possible to differentiate brain tumor from normal tissue [9], [16]–[19] with such dual modality. By investigating the steady-state autofluorescence and diffuse reflectance features of *in vivo* brain tumors, Lin *et al.* showed that such methods are effective in differentiating normal cortex from brain tumors. High sensitivity (up to 100%) and moderate specificity (up to 76%) was obtained in differentiating infiltrating tumor margins from normal brain tissues [9], [16]. In a more recent study on animal, Butte *et al.* also showed that steady-state fluorescence of Indocyanine green prior injected to glioma and normal brain tissue was captured and differentiated with the aid of BLZ-100 and charge-coupled device camera [20]. Valdes *et al.* presented a quantitative and spectral resolved fluorescence imaging approach [21]. This method successfully corrected the emitted fluorescence signals based on the tissue’s optical

Manuscript received July 31, 2015; revised November 10, 2015; accepted December 15, 2015. This work was supported in part by the Natural Sciences and Engineering Research Council of Canada (NSERC Strategic Project), Canada Foundation for Innovation, Ontario Centres of Excellence (OCE Champions of Innovation Program), and Ontario Ministry of Research and Innovation.

Z. Nie is with the School of Biomedical Engineering, McMaster University, Hamilton, ON L8S 4L8, Canada (e-mail: niez2@mcmaster.ca).

V. N. Du Le, D. Cappon, J. E. Hayward, T. J. Farrell, and M. S. Patterson are with the Department of Medical Physics and Applied Radiation Sciences, McMaster University, Hamilton, ON L8S 4L8, Canada (e-mail: ledvn@mcmaster.ca; cappond@mcmaster.ca; JHayward@hhsc.ca; TFarrell@hhsc.ca; MPatters@hhsc.ca).

J. Provias is with the Department of Pathology and Laboratory Medicine, DeGroote School of Medicine, McMaster University, Hamilton, ON L8S 4L8, Canada (e-mail: provijoh@hhsc.ca).

N. Murty is with the Division of Neurosurgery, Department of Surgery, DeGroote School of Medicine, McMaster University, Hamilton, ON L8S 4L8, Canada (e-mail: nkmur10@rogers.com).

W. McMillan is with the Department of Oncology, DeGroote School of Medicine, McMaster University, Hamilton, ON L8S 4L8, Canada (e-mail: mcmillanw@hhsc.ca).

Q. Fang is with the Department of Engineering Physics, School of Biomedical Engineering, McMaster University, Hamilton, ON L8S 4L8, Canada (e-mail: qiyin.fang@mcmaster.ca).

Color versions of one or more of the figures in this paper are available online at <http://ieeexplore.ieee.org>.

Digital Object Identifier 10.1109/JSTQE.2015.2510964

properties. Therefore, it is possible to obtain the absolute fluorophore concentration that can be used for accurate brain tumor detection [21].

Comparing to steady-state fluorescence spectrum, fluorescence lifetime is independent of the emission wavelength, and is sensitive to the microenvironments (e.g., pH, temperature, and ionization). Butte *et al.* used a time-resolved spectroscopic technique to show that normal cortex and normal white matter had longer fluorescence life-time at emission peak 390 nm than that at emission peak 460 nm, and that the method has potentials to classify low-grade gliomas with 100% sensitivity and 98% specificity [10], [11]. However, the slow data acquisition speed ($\sim 40\text{--}60$ s/spot) of previous time-resolved systems prohibited its integration into most clinical settings [10], [11]. In order to evolve time-resolved technology into a practical tool for diagnostic specialists, the new system needs to be much faster with higher temporal resolution, and far more compact and reliable.

Combination of time-resolved fluorescence (TRF) and diffuse reflectance spectroscopy can enable collection of much more contrast features including morphology, functions, and biochemical compositions. The fluorescence emission and laser excitation are altered by tissue's absorption and scattering properties when the light transmits through the biological tissue [22], [23]. The diffuse reflectance signals can be used to compensate this distortion and to retrieve intrinsic fluorescence signals from measured fluorescent signals [24], [25]. Therefore, it is possible to improve the diagnostic accuracy by combine the TRF and diffuse reflectance modality together.

In this paper, we reported an integrated time-resolved fluorescence and diffuse reflectance (TRF-DR) spectroscopy instrument towards the intraoperative detection of brain tumor margin. An acousto-optic-tunable-filter (AOTF)-based spectrometer was used to acquire fluorescence decay signals; a grating-based spectrometer was used to acquire steady-state fluorescence spectra; and a spatial-resolved diffuse reflectance spectroscopy system was used to collect diffuse reflectance spectra in UV-VIS spectral range. A clinical compatible dual-modality fiber-optic probe was used to ensure to collect fluorescence and diffuse reflectance signals at the same location. TRF and DR signals can be acquired within two seconds, which made this system is compatible with neurosurgery. The system performance was validated on standard fluorescence dyes, tissue phantoms, and brain tumor specimens. The results demonstrated that the integrated TRF-DR spectroscopy system can accurately retrieve the fluorescence and optical properties features, thus it has a potential to be used for intraoperative detection for brain tumor margin.

II. METHODS

A schematic of TRF-DR spectroscopy system is illustrated in Fig. 1(a). The integrated system consists of four modules: the TRF subsystem, the DR subsystem, the dual-modality fiber optic probe, and the control unit. The TRF subsystem used a high throughput AOTF-based spectrometer to collect dynamic fluorescence decay signals at different wavelengths. A grating-based spectrograph was also been used to collect steady-state fluorescence spectra. The DR subsystem collected spatially

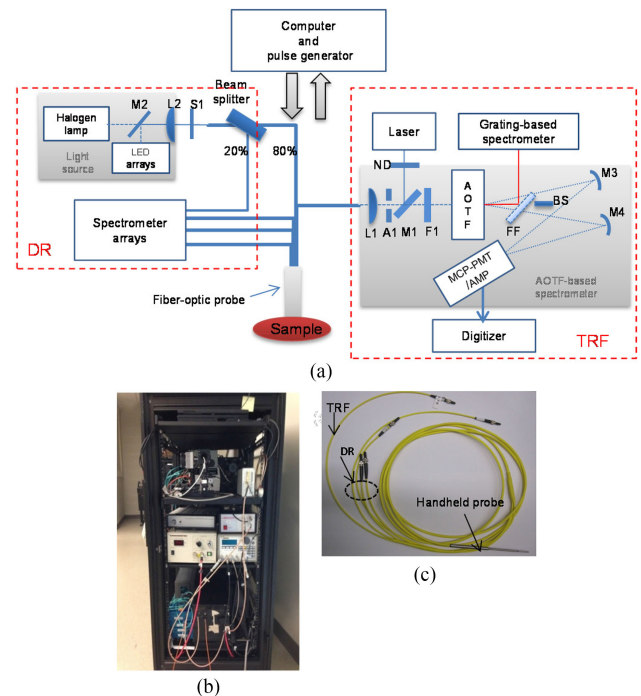


Fig. 1. (a) The schematic view of an integrated TRF-DR spectroscopy system. The system includes four parts: the TRF module, the DR module, the multi-modality fiber optic probe, and the control system. AOTF: acousto-optical tunable filter, MCP-PMT: micro-channel plate photomultiplier tube, AMP: preamplifier, A1: aperture, L1 and L2: plano-convex lens, M1 and M2: dichroic mirrors, M3 and M4: plano-concave mirrors, F1: long-pass filter, S1: shutter, FF: mirror flipper, BS: beam stop, and ND: neutral density filter. (b) TRF-DR spectroscopy instrument housed in a mobile cart. (c) Dual-modality clinical sterilizable fiber optic probe that is used to collect TRF and DR signals.

resolved diffuse reflectance spectra in a small tissue volume. A four-meter long clinical sterilizable fiber optic probe was used to deliver illumination light and to collect TRF and DR signals. Photographs of TRF-DR spectroscopy instrument housed in a mobile cart ($L \times W \times H$: $32 \times 24 \times 50$ inches) and the dual-modality fiber optic probe are shown in Fig. 1(b) and (c), respectively. During clinical studies, autofluorescence and diffuse reflectance signals can be collected in sequence within 2 s.

A. TRF-DR Spectroscopy Instrument Design and Calibration

In the TRF spectroscopy subsystem, a Nd:YAG laser (PNV-001525-140, Teem Photonics, Meylan, France) at 355 nm with 300 picoseconds (ps) pulse width and 1 kHz repetition rate was used as the excitation light source. The laser beam was attenuated by a neutral density filter (ND03A, Thorlabs, Newton, NJ, USA) and a custom-made dichroic mirror (CS0238, Lightwaves 2020, Inc., Milpitas, CA, USA) with 70% reflection at 355 nm at 45° incident angle. The laser beam was then focused into the proximal end of a fused silica optical fiber with a core diameter of $400 \mu\text{m}$ and numerical aperture (NA) of 0.12 by a plano-convex lens. The laser pulse energy on the sample was adjusted to $3 \mu\text{J}$ to avoid photobleaching.

After laser excitation, fluorescence was collected by the same optical fiber and then collimated by the plano-convex lens to a 6 mm diameter beam. An aperture with 6 mm diameter was

mounted after the plano-convex lens to block dispersed fluorescence light. The fluorescence beam transmits through the dichroic mirror (transmission >90% at 370 to 550 nm) and a long-pass filter (OD > 6 at 355 nm, LP02-355RU-25, Semrock, Rochester, NY) to block the backscattered laser light before it reached the AOTF (TEAF5-0.36-0.52-S, Brimrose, Baltimore, MD, USA). A selected spectral band of the collimated fluorescence beam was separated into the ordinary and extraordinary polarized beams which were diffracted toward two concave mirrors, respectively. The non-diffracted light passed through the AOTF and was blocked by a beam stop. Both diffracted beams at the opposite sides of the non-diffracted beam were reflected by concave mirrors (M3 and M4) and then were detected by a fast-gated microchannel plate - photomultiplier tube (MCP-PMT, R5916-50, rise time: 180 ps, Hamamatsu Photonics, Japan). The output signal from the MCP-PMT was amplified with a preamplifier (gain: 63 dBm, bandwidth: 50 KHz–1.5 GHz, C5594-12, Hamamatsu Photonics, Japan) and then digitized by a high speed digitizer (ADQ412, 12 bit, 3.6 GS/s, 1.3 GHz bandwidth, SP Devices, Sweden). A pulse generator (QC9512, Quantum Composer, Bozeman, MT, USA) was used to synchronize the laser and MCP-PMT gate to ensure that the fluorescence decay could be collected within the PMT gating-window. It took the AOTF less than 20 μ s to switch the selected wavelength. Therefore, fluorescence decay signals in the wavelength range of 370–550 nm could be collected rapidly. Due to the bandwidth limitation of the AOTF, a grating-based spectrometer was included to collect the fluorescence spectrometer as well. After time-resolved data acquisition completes, a motorized flip mirror (MFF001, Thorlabs, Newton, NJ, USA) redirected the fluorescence beam to a grating-based spectrometer (BLUEwave, StellarNet, Tampa, FL, USA) as the red solid line shows in the Fig. 1(a), to acquire steady-state fluorescence spectrum. The optical components of the TRF subsystem were shielded in a black enclosure to minimize ambient light.

The AOTF-based spectrometer design and calibration was described in details elsewhere [26], [27]. Briefly, dual-beam configuration was implemented to increase system throughput. The spectra resolution of AOTF-based spectrometer was characterized to be 2.5 nm and its temporal response is \sim 500 ps. The steady state fluorescence spectra collected by the grating-based spectrometer were calibrated by a standard calibration light source (HL-2000-CAL, Ocean Optics, Dunedin, FL, USA) and could be calculated by:

$$F(\lambda) = (F_{\text{measured}}(\lambda) - F_{\text{bkg}}(\lambda)) / S(\lambda). \quad (1)$$

In (1), $F_{\text{measured}}(\lambda)$ is the measured fluorescence spectrum by spectrometer, $F_{\text{bkg}}(\lambda)$ is background noise without laser excitation, and $S(\lambda)$ is spectral correction factor which is the ratio of measured spectra of calibration lamp and standard spectra of the calibration lamp [28].

B. DR Subsystem

In the DR spectroscopy subsystem, a spatially resolved DR spectroscopy subsystem was developed to investigate the optical properties of biological tissues (see Fig. 1(a)). In order to measure the optical properties in the UV-VIS wavelength

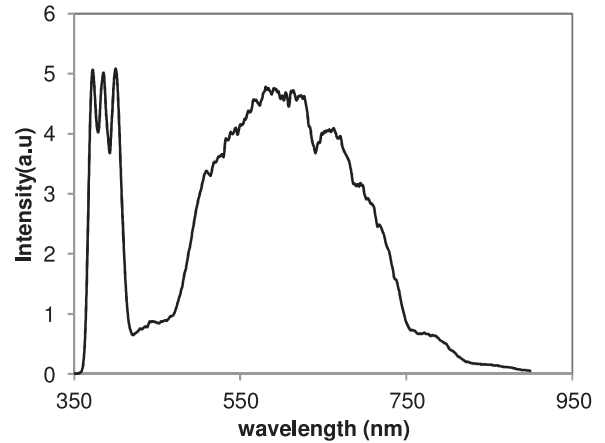


Fig. 2 The spectrum of the broadband light source

range, three high-power UV LEDs (370, 385, and 400 nm, LumiBright, Innovation Optics, Woburn, MA, USA) and a 150 W tungsten-halogen lamp (MI-150, Edmund Optics, Barrington, NJ, USA) were combined into a beam using a dichroic mirror (DLMP425, Thorlabs, NJ, USA) with the cutoff wavelength at 425 nm. The spectrum of the broadband light source is shown in Fig. 2. The combined light beam was split by a 20/80 beam splitter (FOS-400-0102-80/20-123, Fibersense and Signals, San Jose, CA, USA). Twenty percent of the light was used as a reference light; the rest of the light illuminated the sample via a 200 μ m core optical fiber. In addition, a shutter was mounted before the optical fiber coupler to control the light illumination. Four independent spectrometers (BLUEwave, StellarNet, Tampa, FL, USA) were used to collect the reference light and diffuse reflectance spectra at three different source-detector distances (SDDs). This configuration allows setting the integration time for each channel individually to obtain sufficient signals without any optical attenuator, making the system much easier to control during clinical studies.

The background noise was measured and subtracted from measured DR spectra. These spectra were then normalized by the reference light to obtain intensity variation over the measured spectral range. The total diffuse reflectance R from the sample was calculated as:

$$R(\lambda) = (I_m(\lambda) - I_{\text{bkg}}(\lambda)) / (I_{\text{ref}}(\lambda) - I_{\text{bkg}}(\lambda)). \quad (2)$$

In (2), I_{ref} is the measured reflectance intensity of the calibrated diffuse reflectance standard with 99% reflectivity, I_{bkg} is the background noise intensity, and I_m is the measured diffuse reflectance intensity of the sample.

C. Dual-Mode Optical Fiber Probe

A dual-modality fiber optic probe was designed to collect fluorescence and diffuse reflectance signals from the same tissue volume. A schematic view of the probe tips is shown in Fig. 3(a). An optical fiber with a core diameter of 400 μ m and NA of 0.12 was placed at the center of probe. It is used for the laser excitation and fluorescence collection of the TRF subsystem. An optical fiber with a core diameter of 200 μ m and NA of 0.22 placed at the side of probe tips (red dot in figure) is used as the

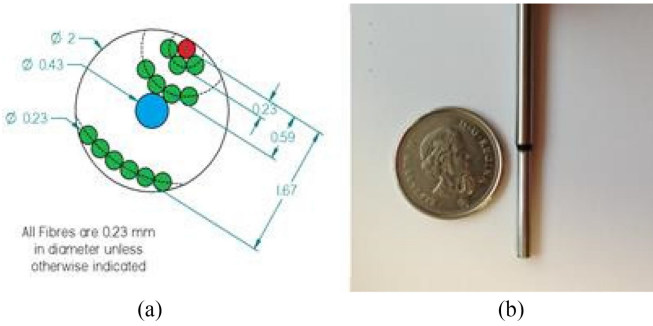


Fig. 3 Dual-modality fiber optic probe. (a) The schematic view of fiber optic probe tip. DR source fiber was placed as red circle shows for a broadband illumination at 355–800 nm. DR detector fibers were arranged in three bundles at the different SDDs as green circles show, while blue indicates the TRF fiber [28]. (b) The photograph of the probe that can be held by the surgeon to collect signals in surgery.

light source for the DR subsystem. The other three fiber bundles is used to collect the DR signals at three SDDs of 0.23, 0.59, and 1.67 mm. The arrangement of fibers was designed using the Monte Carlo simulation to accurately recover the optical properties from tissue [29]. The diameter of the fiber probe is 2 mm as shown in Fig. 3(b). A neurosurgeon can hold the tip of the probe by hand to measure TRF and DR signals during surgery. The fiber probe is in direct contact with the sample surface during measurements.

D. Signal Acquisition and Processing

A program written in Visual C++ was developed to automate the data acquisition process. The precise timing of the data collection sequence was controlled by the pulse generator. For the TRF data collection reported here, fluorescence decays were collected in the spectral range of 370–550 nm with 5 nm intervals. Ten pulses were averaged at each wavelength. Once fluorescence signals are collected, the pulse generator switches to the DR mode to collect diffuse reflectance spectra.

After data acquisition, the raw data were processed in an off-line program. The fluorescence lifetime and intensity were extracted from the decay signals by using the Laguerre-based deconvolution method for fast time-domain parameter estimation [30]. In order to improve the accuracy of the Laguerre-based deconvolution, a constraint was introduced to optimize the linear regression fitting [31]. The average lifetime τ_{avg} was calculated in (3) using the intrinsic response function obtained from Laguerre-based deconvolution method

$$\tau_{\text{avg}} = \left(T \cdot \sum_{n=0}^K k \cdot h(k) \right) / \left(\sum_{n=0}^K h(k) \right). \quad (3)$$

In (3), K is the data length of the decay curve, T is the sampling time interval, and $h(k)$ is the intrinsic fluorescence decay. The intensities at different wavelengths were obtained by integrating the signals over the decay time. In addition, the steady-state spectrum can also be measured from the grating-based spectrometer. The optical properties of the sample were roughly estimated by using an experimental look-up table method [32].

In addition, an optimization method was used to fit the extracted data to obtain the final absorption coefficients and reduced scattering coefficients [33].

E. Clinical Layout and Safety

The TRF-DR spectroscopy system was housed in a mobile cart as shown in Fig. 1(b). An uninterruptible power supply (APC Back-UPS XS1500VA, American Power Conversion, West Kingston, RI, USA) and a medical isolation transformer (ISB-120C, Toroid Co., Salisbury, MD, USA) were used to meet operating room equipment power requirements. In addition, six fans were used to provide sufficient ventilation inside the cart. The fiber probe was sterilized before the surgery. The laser energy was measured by a power meter before clinical studies and adjusted to 3 μJ to avoid the photobleaching and potential thermal damage of biological tissue [34]–[36].

III. MATERIALS

A. Endogenous Biomolecule

To evaluate the ability of TRF subsystem to detect the endogenous fluorescence signals from biological tissue, β -Nicotinamide adenine dinucleotide reduced disodium salt hydrate (NADH, N8129, Sigma-Aldrich, St Louis, MO, USA), flavin adenine dinucleotide disodium salt dehydrate (FAD, F6625, Sigma-Aldrich, St Louis, MO, USA), and collagens type I (C3511, Sigma-Aldrich, St Louis, MO, USA) were measured. The NADH and FAD were dissolved in 10^{-5} M phosphate buffered saline (PBS) solutions individually. The collagen was measured in powdered form. All samples were kept refrigerated before and after measurement.

B. Tissue Phantoms

A series of tissue-simulating liquid phantoms was prepared to investigate the effects of optical properties on the fluorescence measurements. Intralipid (20%, Baxter Corp, Toronto, Canada) was used as a scattering material while black India ink (Higgins, Chartpak, Inc., MA, USA) was used as the absorber. Both were diluted by deionized water to obtain different concentrations.

In order to investigate the effect of the scattering properties on the fluorescence spectral and lifetime measurements, a phantom group was prepared with the same absorption coefficient but different scattering coefficients. The India ink with a concentration of 0.003% v/v was used for each phantom to obtain a constant absorption coefficient of 0.02 mm^{-1} . The Intralipid concentration of 1% v/v, 1.2% v/v, and 1.4% v/v were used in different phantoms corresponding to the reduced scattering coefficients of 1.5, 1.8, and 2.1 mm^{-1} at 515 nm. Fluorescein (46955-100G-F, Sigma-Aldrich, MO, USA) with an emission peak at 515 nm and an average lifetime of 4.1 ns was added into these liquid phantoms to obtain a concentration of 0.1 mM. The optical properties of the fluorescent phantoms were measured after adding the fluorescein dye. Autofluorescence signals of Intralipid in tissue phantoms have also been studied in our previous studies [37]. The results shows that autofluorescence of Intralipid can be neglected in these tissue phantoms.

C. Brain Tumor

Brain tumor samples obtained from patients undergoing tumor resection surgery at the Hamilton General Hospital, Hamilton, Canada were investigated by using the developed TRF-DR spectroscopy system. The research protocol and consent was approved by the Hamilton Health Sciences/McMaster Research Ethics Board. The brain specimens taken from the patient at surgery were investigated within one hour after excision. During experimental measurements, the sample was kept in a petri dish and soaked in saline (PH: 5.5) to keep moist. After measurements, the samples were stored in the buffered formalin for pathological examination.

IV. RESULTS

A. Fluorescence Characteristics of Endogenous Biomolecules

The capability of the TRF subsystem in resolving the endogenous fluorescence was validated by measuring the biological molecules including NADH, FAD, and Collagen type I. The fluorescence spectra were integrated from the TRF decay signals. The fluorescence decay curves were fitted by the Laguerre-based deconvolution method and exponential-based deconvolution method to retrieve intrinsic response functions. The fluorescence spectra and lifetime of the biomolecules are shown in Fig. 4. NADH had a broadband emission spectrum from 380 to 550 nm with an emission peak at 450 nm and lifetime of 0.61 ns, while FAD had relatively narrow emission spectrum above 500 nm with an emission peak at 520 nm and lifetime of 2.91 ns. Collagen also had a broadband emission spectrum with the emission peaks around 440 nm. The lifetime of collagen decreased quickly in longer wavelength. As shown in Table I, the lifetime values of the biological molecules agreed with the previous studies [28], except that the NADH had higher value than reported results, which was limited by the temporal resolution of the TRF subsystem. However, NADH is usually bonded with protein in cells or tissue. The lifetime of NADH changes according to its bonding status. For example, the fluorescence lifetime of NADH in mitochondria (2.8 ns) was much longer than that of pure solution (0.43 ns) [5]. Therefore, the TRF subsystem is capable of retrieving the NADH component from biological tissue. Collagen usually has short and long lifetime components that can be observed from the bi-exponential fitting results. These results indicated that our TRF subsystem is able to retrieve both spectrum and lifetime of endogenous fluorophores in the biological tissue.

B. Effects of Optical Properties on Fluorescent Signals

To investigate the effect of the scattering property on the fluorescence, the fluorescence spectra and decays were collected from the tissue-simulating phantoms. The steady-state fluorescence spectrum measured from grating-based spectrum, and normalized decay curve of each phantom are shown in Fig. 5. In addition, Fluorescein's spectra integrated from time resolved decay signals keep consistent with results from grating-based spectrometer. It is observed that the spectral shape did not change with the reduced scattering coefficient, while the fluorescence

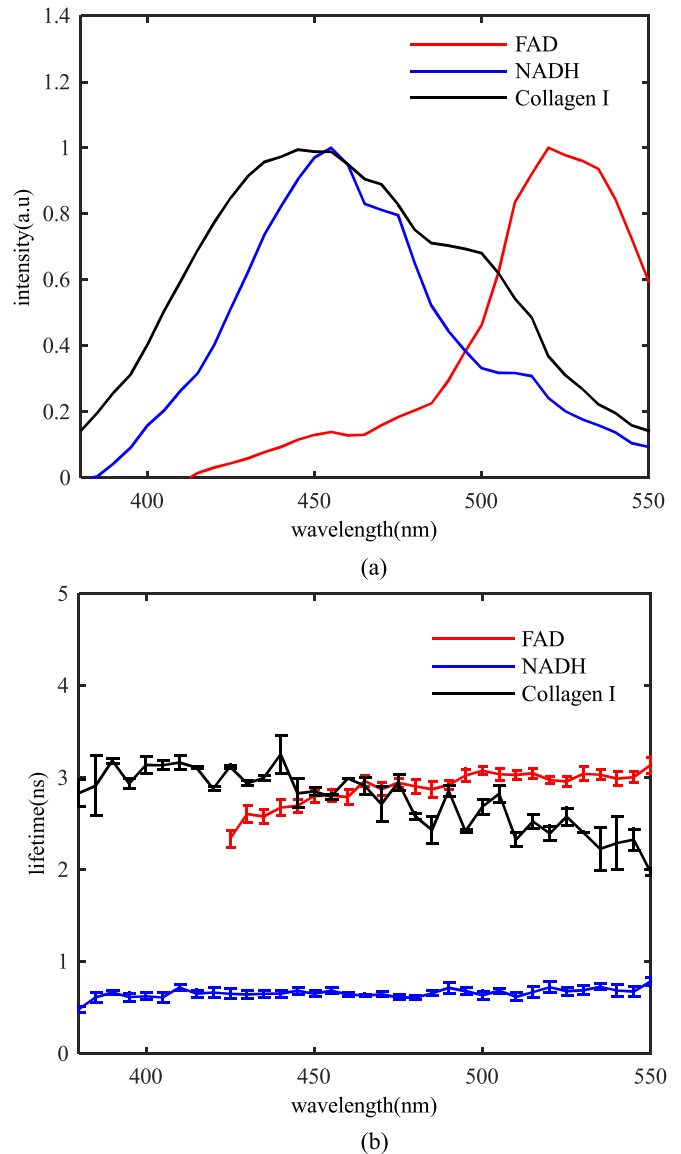


Fig. 4. System characterization on biological molecules fluorophores. (a) The spectra of NADH, FAD, and Collagen with the emission peak at 450, 520, 445 nm, respectively. (b) The lifetime values for different biological molecules fluorophores over the observed spectral range (data: mean \pm standard error).

intensity decreased with the increase of the reduced scattering coefficient. The calculated lifetime values from the fluorescence decay curves are summarized in Table II. The lifetime values remain constant over the reduced scattering coefficients. The effect of the absorption on the fluorescence measurement was also investigated. With the increase of absorption coefficients, the fluorescence intensity decreased gradually, whereas the fluorescence decays did not change (figures are not shown). These experimental results demonstrates that fluorescence lifetime does not change with optical properties when using a single optical fiber for illumination and fluorescence collection, whereas the fluorescence spectra were altered by the scattering and absorption properties. These results are in good agreements with Vishwanath *et al.*'s results in which a Monte Carlo model was used to simulate the fluorescence transmission in the turbid

TABLE I
ENDOGENOUS FLUOROPHORES LIFETIME MEASUREMENT

Samples	Peak wavelength	Lifetime (ns)		Reference [28]
		Laguerre	Exponential-based	
FAD	520 nm	2.96 ± 0.10	2.81 ± 0.08	2.3 ~ 2.86
NADH	450 nm	0.61 ± 0.09	0.58 ± 0.12	0.3 ~ 0.4
Collagen	440 nm	2.76 ± 0.12	1.01 ± 0.11 5.07 ± 0.28	0.6 4.9

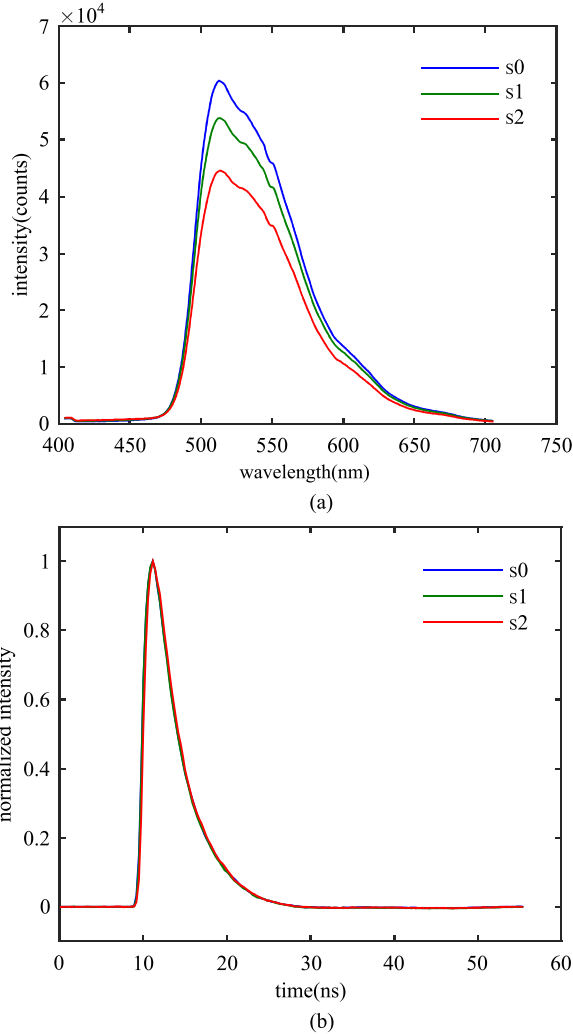


Fig. 5. The fluorescence signals measured from tissue phantoms with same absorption property but different scattering properties. (a) Fluorescence emission spectra from different phantoms (S0, S1, and S2). (b) Fluorescence decays are normalized at the peak emission.

tissue with various optical properties [23]. Therefore, only the distortion of the fluorescence spectra needs to be corrected from measured fluorescence signals in our future studies.

C. Ex Vivo Measurements of Brain Tumor Specimens

Brain tumor specimens were measured by the TRF-DR spectroscopy to investigate their fluorescence and optical properties.

TABLE II
FLUORESCENCE LIFETIME ESTIMATION FOR THE TISSUE PHANTOMS WITH DIFFERENT REDUCED SCATTERING COEFFICIENTS

Phantom	Optical properties at 515 nm		Fluorescein concentration (mMol)	Lifetime (ns)
	μ'_s (mm ⁻¹)	μ_a (mm ⁻¹)		
s0	1.5	0.02	0.1	4.1 ± 0.1
s1	1.8	0.02	0.1	4.0 ± 0.1
s2	2.1	0.02	0.1	4.0 ± 0.1

Fig. 6 shows the results of an *ex vivo* clinical study of the brain tumor specimen. The measured tumor sample is shown in Fig. 6(a). The sample was investigated in one hour after resection from surgery. The measured spot was marked using the green biological dye (Davidson Marking system, Bradley Products, Inc., Minneapolis, MN, USA) for further pathological diagnosis. The fluorescence spectra and lifetime measured by TRF spectroscopy are shown in Fig. 6(b) and (c), respectively. The brain tumor specimen had the maximum fluorescence emission at 455 nm which is through to be mainly contributed by NADH. Another emission peak at 520 nm may be mainly contributed by FAD. The lifetime increases from 370 to 550 nm. This is likely due to the spectral distribution of different fluorophores in the tissue sample. For example, collagen fluoresces in 370–440 nm region with shorter lifetime (average of 4–5 ns). The binding form of the NADH also have a higher lifetime which contribute to overall lifetime change in the wavelength range of 400 to 500 nm, while flavin mononucleotide (FMN) fluoresces in 510–520 nm region with longer lifetime (average of 6–10 ns) [39], [40]. The total diffuse reflectance spectra and optical properties are shown in Fig. 6(d) and (e), respectively. Due to strong blood absorption in the wavelength range of 400–450 nm [38], reflectance signal in this region was too weak to be used for recovering of optical properties. Therefore, only reflectance in 450–700 nm was used. The diffuse reflectance was calculated using Eq. (2) while the optical properties were predicted using a look-up table based method coupling with fitting algorithms. A similar LUT and fitting approach can also be found in earlier studies [31], [32]. Fig. 6(d) shows the total diffuse reflection collected with the closest fibers (SDD = 0.23 and 0.59 mm). Signal to noise ratio is poor at SDD of 1.67 mm, especially at high absorptive wavelengths such as 450, 540 and 580 nm. Therefore, only diffuse reflectance measurements at SDD of 0.23 and 0.59 mm were used to recover optical properties and were shown in Fig. 6(d). Fig. 6(e) shows the corresponding predicted optical properties using the LUT and fitting methods which have average errors of less than 10% on simulated hemoglobin (H0267, Sigma-Aldrich, MO, USA) phantoms.

V. DISCUSSION AND CONCLUSION

An integrated TRF-DR spectroscopy instrument was developed for *in vivo* and *ex vivo* optical biopsy studies. The fluorescence and diffuse reflectance signals can be collected rapidly within two seconds using a custom-made clinical sterilizable fiber optic probe.

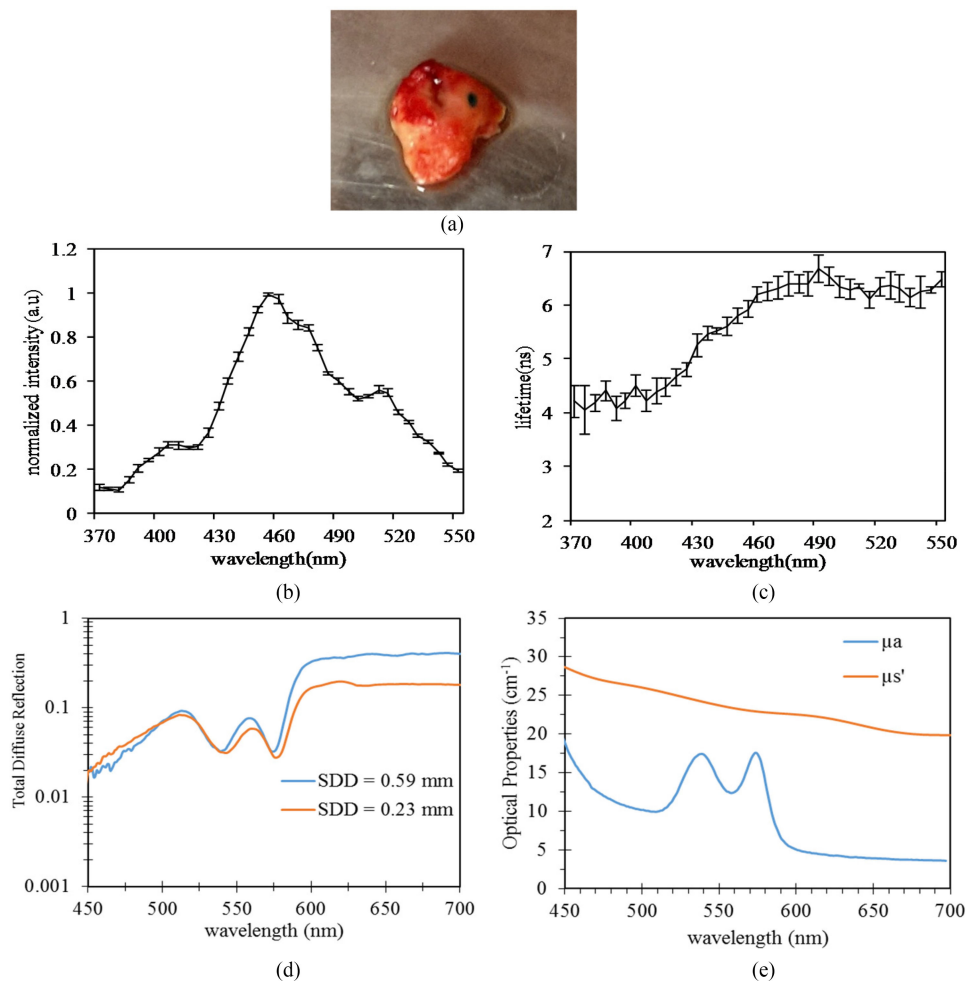


Fig. 6. An *ex-vivo* clinical study results of brain tumor specimen using the TRF-DR spectroscopy system. (a) the photograph of brain tumor sample, (b) fluorescence spectrum, (c) fluorescence lifetime, (d) spatial resolved diffuse reflectance spectra at different SDDs (0.23 mm and 0.59 mm), (e) optical properties (μ_a : absorption coefficient and μ_s' : reduced scattering coefficient). (data : mean \pm standard error).

In the TRF subsystem, spectral resolved capability was realized by using an AOTF-based spectrometer to switch the diffracted wavelength within several microseconds. This configuration dramatically reduces the data acquisition time compared to the grating-based system used in previous study [27]. Even though two diffracted beams have slight differences in the peak wavelength, which are limited by the AOTF crystal's configuration and properties; it is still within the tolerance of our study since the spectral resolution is around 5 nm for fluorescence measurements. Moreover, comparing to band-pass filters that are used to collect signals in limited spectral bands, this design allows for choosing the interested wavelength by changing the RF frequency applied on AOTF without any physical modification. This ensures that the current system is more robust to choose the different wavelengths of interest based on the clinical study requirement. In the DR subsystem, the broadband light source was designed by combining the UV LEDs and the halogen lamp, which allows us to observe the diffuse reflectance spectra in the UV-VIS spectral range for calibration with ink phantoms. However, the *ex vivo* sample's reflectance signals in the UV range could not be measured with these LEDs due to strong blood absorption [38]. Four independent spectrometers

were used to acquire the spatial resolved diffuse reflectance spectra from different SDDs and reference light. This configuration allows adjusting the diffuse reflectance light intensity for each channel individually and quickly. The dual-modality optical fiber probe was designed and fabricated to retrieve the optical properties accurately from the diffuse reflectance spectra in a small tissue volume. Meanwhile, it also ensures to collect the TRF and DR signals at same location.

The system performances were validated using the standard fluorescent biomolecules, tissue phantoms, and *ex vivo* brain tumor specimen. Both biochemical and morphological information can be investigated according to the TRF and DR measurements. The system is able to obtain multiple contrast features. Fluorescence signals are altered by tissue absorption and scattering properties as shown in Fig. 5, this influences the accuracy of diagnosis. In the *ex vivo* brain tumor study as Fig. 6 shows, we are not able to obtain the optical properties in the UV range due to the low reflectance signals. This is caused by strong blood absorption and low LED intensity. In future, the high power LED light source will be used to increase reflectance signal intensity. In addition, the autofluorescence from GBM is mainly contributed by NADH and FAD which have the emission peaks

at 450 and 520 nm respectively [11]. In a future manuscript, an experimental approach will be developed to recover fluorescence from the measured optical properties, diffuse reflectance, and steady state fluorescence. Careful evaluations of such approach will be performed on tissue simulating phantoms before it can be applied to tissue measurements. During the clinical studies, the diffuse reflectance signals of the 355 nm laser light source will also be measured to determine the optical properties and penetration depth of the excitation light. In future, new algorithms will be developed to extract the intrinsic fluorescence signals based on these measurement results.

In summary, a multi-modalities integration system was built to acquire time-resolve fluorescence and diffuse reflectance signals in real-time, which is compatible to intraoperative brain tumor diagnosis during the surgery. The system was calibrated and validated by the fluorescence bio-molecules, tissue phantom and *ex vivo* brain tumor study. It is capable to retrieve the fluorescence signals as well as the optical properties from the brain tumor sample. The system will be used for *in vivo* clinical study to investigate the fluorescence and diffuse reflectance characteristics of brain tumors. Furthermore, the classification methods will be developed to differentiate the brain tumor from normal tissue based on the *in vivo* clinical study results.

REFERENCES

- [1] R. Siegel, J. Ma, Z. Zou, and A. Jemal, "Cancer statistics 2014," *Cancer J. Clin.*, vol. 64, no. 1, pp. 9–29, 2014.
- [2] Central Brain Tumor Registry of the United States, "CBTRUS statistical report: Primary brain and central nervous system tumors diagnosed in the united states in 2004–2008." (2012). [Online]. Available: <http://www.cbtrus.org/>
- [3] Y. Eypoglu, M. Buchfelder, and N. E. Savaskan, "Surgical resection of malignant gliomas—Role in optimizing patient outcome," *Nature Rev. Neurol.*, vol. 9, no. 3, pp. 141–151, 2013.
- [4] N. Sanai *et al.*, "An extent of resection threshold for newly diagnosed glioblastomas: Clinical article," *J. Neurosurgery*, vol. 115, no. 1, pp. 3–8, 2011.
- [5] I. Georakoudi *et al.*, "NAD(P)H and Collagen as *in vivo* quantitative fluorescent biomarkers of epithelial precancerous changes," *Cancer Res.*, vol. 62, no. 3, pp. 682–687, 2002.
- [6] J. D. Pitts *et al.*, "Autofluorescence characteristics of immortalized and carcinogen-transformed human bronchial epithelial cells," *J. Biomed. Opt.*, vol. 6, no. 1, pp. 31–40, 2001.
- [7] V. Lutz *et al.*, "Impact of collagen crosslinking on the second harmonic generation signal and the fluorescence lifetime of collagen autofluorescence," *Skin. Res. Technol.*, vol. 18, no. 2, pp. 168–179, 2012.
- [8] M. C. Skala *et al.*, "In vivo multiphoton microscopy of NADH and FAD redox states, fluorescence lifetimes, and cellular morphology in precancerous epithelia," *Proc. Nat. Acad. Sci. USA*, vol. 104, no. 49, pp. 19494–19499, 2007.
- [9] W. C. Lin *et al.*, "In vivo brain tumor demarcation using optical spectroscopy," *Photochem. Photobiol.*, vol. 73, no. 4, pp. 396–402, 2001.
- [10] P. V. Butte *et al.*, "Fluorescence lifetime spectroscopy for guided therapy of brain tumors," *Neuroimage*, vol. 54, no. 1, pp. 125–135, 2011.
- [11] P. V. Butte *et al.*, "Intraoperative delineation of primary brain tumors using time-resolved fluorescence spectroscopy," *J. Biomed. Opt.*, vol. 15, no. 2, p. 027008, 2010.
- [12] S. Andersson-Engels *et al.*, "Preliminary evaluation of two fluorescence imaging methods for the detection and the delineation of basal cell carcinomas of the skin," *Lasers. Surg. Med.*, vol. 26, no. 1, pp. 76–82, 2000.
- [13] L. Marcu *et al.*, "In vivo detection of macrophages in a rabbit atherosclerotic model by time-resolved laser-induced fluorescence spectroscopy," *Atherosclerosis*, vol. 181, no. 2, pp. 295–303, 2005.
- [14] T. J. Pfefer *et al.*, "Temporally and spectrally resolved fluorescence spectroscopy for the detection of high grade dysplasia in Barrett's esophagus," *Lasers. Surg. Med.*, vol. 32, no. 1, pp. 10–16, 2003.
- [15] N. Lue *et al.*, "Portable optical fiber probe-based spectroscopic scanner for rapid cancer diagnosis: A new tool for intraoperative margin assessment," *PLoS One*, vol. 7, no. 1, p. e30887, 2012.
- [16] W. C. Lin *et al.*, "Diffuse reflectance spectroscopy for *in vivo* pediatric brain tumor detection," *J. Biomed. Opt.*, vol. 15, no. 6, p. 061709, 2010.
- [17] A. Kim, Y. Moriyama, B. C. Wilson, and M. Khurana, "Quantification of *in vivo* fluorescence decoupled from the effects of tissue optical properties using fiber-optic spectroscopy measurements," *J. Biomed. Opt.*, vol. 15, no. 6, p. 067006, 2010.
- [18] M. D. Keller *et al.*, "Autofluorescence and diffuse reflectance spectroscopy and spectral imaging for breast surgical margin analysis," *Lasers Surg. Med.*, vol. 42, no. 1, pp. 15–23, 2010.
- [19] N. Yadav *et al.*, "In vivo detection of epileptic brain tissue using static fluorescence and diffuse reflectance spectroscopy," *J. Biomed. Opt.*, vol. 18, no. 2, p. 27006, 2013.
- [20] P. V. Butte *et al.*, "Near-infrared imaging of brain tumors using the Tumor Paint BLZ-100 to achieve near-complete resection of brain tumors," *Neurosurg. Focus*, vol. 36, no. 2, p. E1, 2014.
- [21] P. A. Valdés *et al.*, "Quantitative, spectrally-resolved intraoperative fluorescence imaging," *Sci. Rep.*, vol. 2, p. 798, 2012.
- [22] M. G. Müller *et al.*, "Intrinsic fluorescence spectroscopy in turbid media: Disentangling effects of scattering and absorption," *Appl. Opt.*, vol. 40, no. 25, pp. 4633–4646, 2001.
- [23] K. Vishwanath, B. Pogue, and M. A. Mycek, "Quantitative fluorescence lifetime spectroscopy in turbid media: comparison of theoretical, experimental and computational methods," *Phys. Med. Biol.*, vol. 47, no. 18, pp. 3387–3405, 2002.
- [24] A. Kim, M. Khurana, Y. Moriyama, and B. C. Wilson, "Quantification of *in vivo* fluorescence decoupled from the effects of tissue optical properties using fiber-optic spectroscopy measurements," *J. Biomed. Opt.*, vol. 15, no. 6, p. 067006, 2010.
- [25] K. Vishwanath and M-A. Mycek, "Time-resolved photon migration in bilayered tissue models," *Opt. Exp.*, vol. 13, no. 19, pp. 7466–7482, 2005.
- [26] Y. Yuan *et al.*, "High-throughput acousto-optic-tunable-filter-based time-resolved fluorescence spectrometer for optical biopsy," *Opt. Lett.*, vol. 34, no. 7, pp. 1132–1134, 2009.
- [27] Z. Nie *et al.*, "Hyperspectral fluorescence lifetime imaging for optical biopsy," *J. Biomed. Opt.*, vol. 18, no. 9, p. 096001, 2013.
- [28] Q. Fang *et al.*, "Time-domain laser-induced fluorescence spectroscopy apparatus for clinical diagnostics," *Rev. Sci. Instrum.*, vol. 75, no. 1, pp. 151–162, 2004.
- [29] D. J. Cappon *et al.*, "Fiber-optic probe design and optical property recovery algorithm for optical biopsy of brain tissue," *J. Biomed. Opt.*, vol. 18, no. 10, p. 067006, 2013.
- [30] J. Jo *et al.*, "Fast model-free deconvolution of fluorescence decay for analysis of biological systems," *J. Biomed. Opt.*, vol. 9, no. 4, pp. 743–752, 2004.
- [31] J. Liu, Y. Sun, J. Qi, and L. Marcu, "A novel method for fast and robust estimation of fluorescence decay dynamics using constrained least-squares deconvolution with Laguerre expansion," *Phys. Med. Biol.*, vol. 57, no. 4, pp. 843–865, 2012.
- [32] N. Rajaram, T. H. Nguyen, and J. W. Tunnell, "Lookup table-based inverse model for determining optical properties of turbid media," *J. Biomed. Opt.*, vol. 13, no. 5, p. 050501, 2008.
- [33] Q. Wang, V. N. Du Le, J. Ramella-Roman, and J. Pfefer, "Broadband ultraviolet-visible optical property measurement in layered turbid media," *Biomed. Opt. Exp.*, vol. 3, no. 6, pp. 1226–1240, 2012.
- [34] L. Marcu, W. S. Grundfest, and J. M. Maarek, "Photobleaching of arterial fluorescent compounds: Characterization of elastin, collagen and cholesterol time-resolved spectra during prolonged ultraviolet irradiation," *Photochem. Photobiol.*, vol. 69, no. 6, pp. 713–721, 1999.
- [35] *American National Standard for Safe Use of Lasers*, Laser Institute of America ANSI Z136.1-2007, 2007.
- [36] J. A. Zuchlich, "Ultraviolet-induced photochemical damage in ocular tissues," *Health Phys.*, vol. 56, no. 2, pp. 671–682, 1989.
- [37] V. N. Du Le *et al.*, "Measurements of extrinsic fluorescence in intralipid and polystyrene microspheres," *Biomed. Opt. Exp.*, vol. 5, no. 8, pp. 2726–2735, 2014.
- [38] M. Friebe, A. Roggan, G. Müller, and M. Meinke, "Determination of optical properties of human blood in the spectral range 250 to 1100 nm using Monte Carlo simulations with hematocrit-dependent effective scattering phase functions," *J. Biomed. Opt.*, vol. 11, no. 3, p. 034021, 2006.
- [39] M. Y. Berezin and S. Achilefu, "Fluorescence lifetime measurements and biological imaging," *Chem. Rev.*, vol. 110, no. 5, pp. 2641–2684, 2010.
- [40] W. R. Zipfel *et al.*, "Live tissue intrinsic emission microscopy using multiphoton-excited native fluorescence and second harmonic generation," *Proc Nat. Acad. Sci.*, vol. 100, no. 12, pp. 7075–7080, 2003.



Zhaojun Nie received the B.Sc. degree in electrical engineering from Xi'an Post and Communication University, Beijing, China, in 2007, the M.Sc. degree in optoelectronic engineering from the Beijing Institute of Technology, Beijing, in 2009, and the Ph.D. degree in biomedical engineering from McMaster University, Hamilton, ON, Canada, in 2014. She is currently a Postdoctoral Scientist at Cedars-Sinai Medical Center, Los Angeles, CA, USA. Her research interests include biophotonic techniques in clinical research, including time-resolved fluorescence spectroscopy, diffuse reflectance spectroscopy, fluorescence lifetime imaging for clinical diagnosis.

fluorescence lifetime imaging for clinical diagnosis.



Joseph E. Hayward received the Ph.D. degree in lasers and electrooptics in engineering physics from McMaster University, Hamilton, ON, Canada, in 1993. He joined the Biomedical Optics Group, Juravinski Cancer Centre, Hamilton as a Research Associate to assist in the development of optical methods and instrumentation for the diagnosis, staging, and treatment of cancer, as well as the monitoring of cancer treatments. In 1998, he joined the Cancer Centre as a Medical Physicist. He is currently an Associate Professor in the Department of Radiology and the Department of Medical Physics and Applied Radiation Sciences, McMaster University, where he is also an Associate Member of Department of Engineering Physics. He is also a Member of the Canadian College of Physicists in Medicine. His current research interests include optical methods of monitoring radiation-induced toxicities and noninvasive strategies to identify the margins of malignant skin lesions.

the Department of Medical Physics and Applied Radiation Sciences, McMaster University, where he is also an Associate Member of Department of Engineering Physics. He is also a Member of the Canadian College of Physicists in Medicine. His current research interests include optical methods of monitoring radiation-induced toxicities and noninvasive strategies to identify the margins of malignant skin lesions.



Vinh Nguyen Du Le received the B.Sc. and the M.Sc. degrees in biomedical engineering from the Catholic University of America, Washington, DC, USA, in 2009 and 2010, respectively. From 2010 to 2012, he was a Research Fellow at the Optical Diagnostic Devices Laboratory, Center of Radiological Health (CDRH), U. S. Food and Drug Administration. He is currently working toward the Ph.D. degree in the Medical Physics Program, McMaster University, Hamilton, ON, Canada, where his research aims to detect human brain and breast tumor margin using novel optical imaging techniques.

novel optical imaging techniques.



Thomas J. Farrell received the Ph.D. degree in medical physics from McMaster University, Hamilton, ON, Canada, in 1990. He is currently a Medical Physicist at the Juravinski Cancer Centre, Hamilton, and a Professor in the Departments of Radiology and Medical Physics, McMaster University. His current research interests include optical spectroscopy and dosimetry for photodynamic therapy.



Michael S. Patterson received the B.Sc. degree from Queen's University, Kingston, ON, Canada, in 1973, a M.Sc. degree from McMaster University, Hamilton, ON, Canada, in 1976, and the Ph.D. degree from the University of Toronto, Toronto, ON, Canada, in 1984.

He is the Head of medical physics at Juravinski Cancer Centre, Hamilton Health Sciences, and a Professor in the Department of Radiology and the Department of Medical Physics and Applied Radiation Sciences, McMaster University. His current research

interests include photodynamic therapy, optical diagnostics, and quantitative optical imaging.



Derek Cappon received the B.Eng. degree in biomedical and electrical engineering from McMaster University, Hamilton, ON, Canada, in 2008, where he is currently working toward the Ph.D. degree at Medical Physics & Applied Radiation Sciences. He is working as a Health Physicist in the Nuclear Reactor, McMaster University.

John Provias received the M.D. degree from McMaster University, Hamilton, ON, Canada, in 1981 and FRCPC from the University of Toronto, Toronto, ON, Canada, in 1994. He is currently an Associate Professor in the Pathology and Molecular Medicine, McMaster University. He is also the Neuropathologist for Hamilton Regional Cancer Centre. His research interests include Alzheimer's disease and aspects of brain tumor biology.

Naresh Murty received the B.Sc. degree in biology from Dalhousie University, Halifax, NS, Canada, and the M.D. degree from Kasturba Medical College, Manipal, Karnataka, India. He is currently an Associate Professor in the Division of Neurosurgery, McMaster University. He is also the Head of neurosurgery service at Hamilton General Hospital. His research interests include novel therapies for glioblastoma and translational neurosurgical device development.

William McMillan received the B.A. degree from Queen's University, Kingston, ON, Canada, and the B.Sc. and M.Sc. degrees from McMaster University, Hamilton, ON, Canada. He also received the MB.ChB degree from University College, Dublin, Ireland. He is currently an Associate Professor in the Department of Oncology, McMaster University. His research interests include clinical trials investigator, translational neurosurgical device development, and CNS oncology.



Qiyin Fang received the B.Sc. degree in physics from Nunki University, Tianjin, China, in 1995, the M.Sc. degree in applied physics, and the Ph.D. degree in biomedical physics from East Carolina University, Greenville, NC, USA, in 1998 and 2002, respectively. He is currently an Associate Professor of engineering physics at McMaster University, where he also holds the Canada Research Chair in Biophotonics. His current research interests include optical spectroscopy and imaging for minimally invasive diagnosis and guided therapy, miniaturized sensors and imaging systems, and advanced optical microscopy.

imaging systems, and advanced optical microscopy.